Case Studies in Chemical and Environmental Engineering 12 (2025) 101270

Contents lists available at ScienceDirect

Case Studies in Chemical and Environmental Engineering

journal homepage: www.sciencedirect.com/journal/case-studies-in-chemical-and-environmental-engineering

Case Report

The effect of mechanical milling and two-step sintering technique on the microstructure, microhardness, strength, and dielectric properties of $Sm_2Zr_2O_7$ ceramics

I.E. Kenzhina [a,b,c], A.L. Kozlovskiy [a,d], R.I. Shakirzyanov [d,*], M.E. Kaliyekperov [d], N.O. Volodina [d], S.A. Maznykh [d], M. Begentayev [a], S.K. Askerbekov [a,d], Zh.A. Zaurbekova [a,d], A.U. Tolenova [a], P.A. Blynskiy [a]

[a] Satbayev University, Satbayev str.22, Almaty, 050000, Kazakhstan
[b] Kazakh-British Technical University, Tole bi 59 str., Almaty, 050000, Kazakhstan
[c] Institute of Experimental and Theoretical Physics, al-Farabi Kazakh National University, al-Farabi av. 71, Almaty, 050040, Kazakhstan
[d] Engineering Profile Laboratory, L.N. Gumilyov Eurasian National University, Satpayev St. 2, Astana, 010008, Kazakhstan

ARTICLE INFO

Keywords:
Sintering
Ceramics
Grain size
Porosity
Microhardness
Strength

ABSTRACT

This paper investigates the effect of two-step sintering on the mechanical properties and microstructure of $Sm_2Zr_2O_7$ ceramics obtained from submicron powders after high-energy milling. Two key parameters of the two-step sintering process are analyzed: temperature and duration, as both can significantly influence grain growth processes in ceramics. It was found that extending the sintering duration at lower temperatures promotes ceramic densification while preserving a relatively narrow grain size distribution. In contrast, higher sintering temperatures combined with shorter durations result in broader grain size distributions and more pronounced exaggerated grain growth. Despite differences in microstructure and grain size distribution, both the sample sintered at 1350 °C for 20 hours and the one sintered at 1700 °C for 10 minutes exhibited the highest mechanical properties, with microhardness values HV1 ~1200 and biaxial flexural strength reaching ~125 MPa. This suggests that the enhancement of mechanical performance may be linked to a reduction in internal stresses, either due to the elevated temperature during the first sintering step or the extended holding time during the second step. Thus, in both types of sintering, whether based on prolonged holding time or elevated temperature, changes in sample morphology and grain size do not appear to have a significant impact on the mechanical properties of the resulting ceramics.

1. Introduction

Despite the large number of articles dedicated to the fabrication of submicron or nanograin ceramics and the great attention of the ceramic scientific community to pressureless sintering, the problems of high porosity and uncontrolled grain growth remain unresolved [1–7]. Addressing these issues continues to be of great interest to researchers for several reasons. If we list the most important of them, we can highlight the following. Polycrystalline materials with a narrow grain size distribution and an average grain size close to the nanoscale level have excellent mechanical characteristics (compressive strength, bending strength, high hardness), dielectric performance (low dielectric loss, high breakdown voltage values), and corrosion resistance. Obtaining such materials often involves the use of expensive equipment, such as spark plasma sintering [8], high pressure sintering (isostatic or uniaxial compression) [9–11], microwave sintering [12] and other methods. Another important advantage of using nanostructured polycrystalline materials is the potential to lower sintering temperatures and reduce thermal processing times for green bodies prepared from submicron powders or nanoprecursors. Furthermore, such materials are generally easier to process compared to those produced via conventional solid-state synthesis [13]. In addition, a common drawback in ceramic production is the significant variability in the properties of final products from batch to batch, primarily caused by microstructural and chemical heterogeneity. Reducing the grain size can significantly improve the microstructural uniformity and help overcome typical

* Corresponding author.
E-mail address: shakirzyanov_ri@enu.kz (R.I. Shakirzyanov).

https://doi.org/10.1016/j.cscee.2025.101270
Received 20 March 2025; Received in revised form 25 April 2025; Accepted 26 July 2025
Available online 28 July 2025

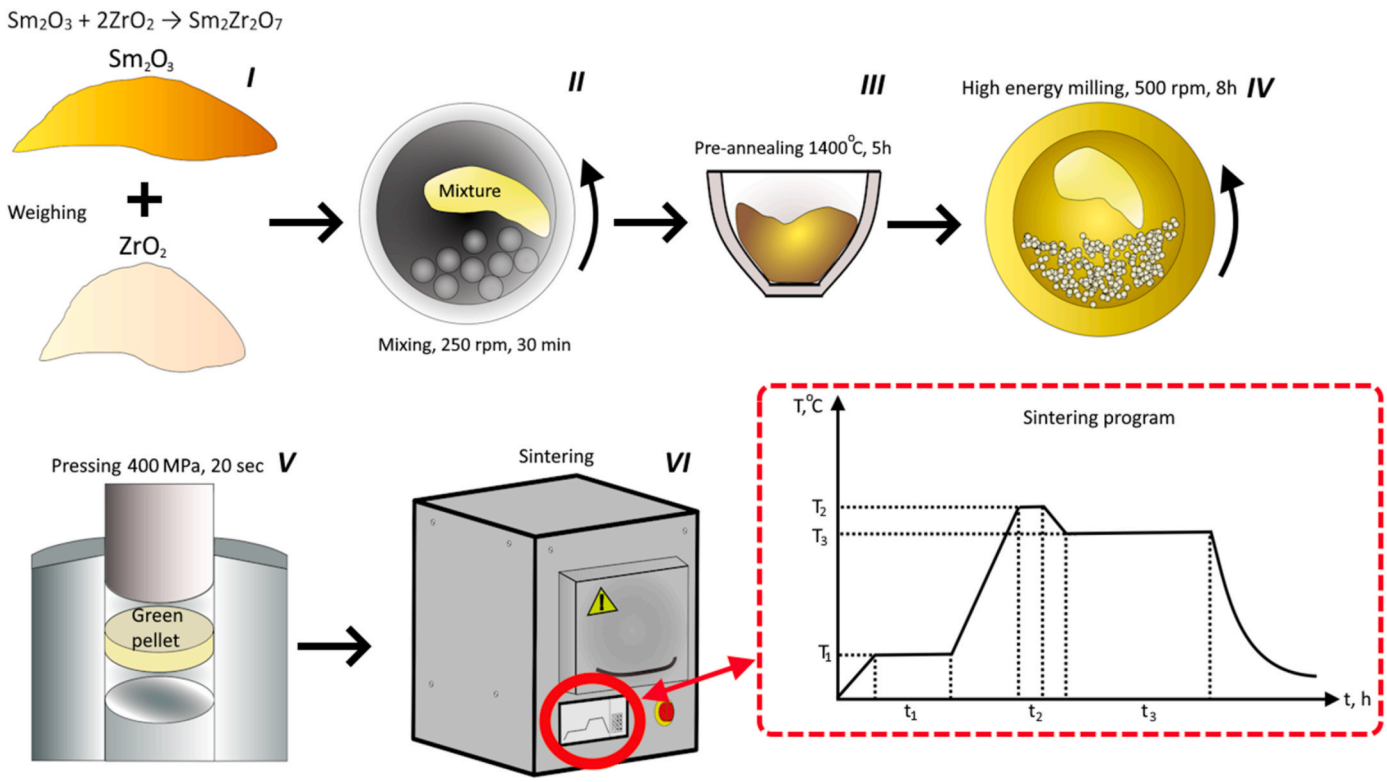

Fig. 1. Schematic graphical representation of experimental samples synthesis.

Table 1
Temperature regimes of experimental samples sintering.

№	Designation	T_1, °C	t_1, h	T_2, °C	t_2, min	T_3, °C	t_3, h
1	OS1300	400	2	–	–	1300	5
2	OS1400	400	2	–	–	1400	5
3	OS1500	400	2	–	–	1500	5
4	TS1350h5	400	2	1450	10	1350	5
5	TS1350h10	400	2	1450	10	1350	10
6	TS1350h20	400	2	1450	10	1350	20
7	TS1600	400	2	1600	10	1500	5
8	TS1700	400	2	1700	10	1500	5

problems in ceramic manufacturing.

In the case of pressureless sintering, a two-step sintering method can be applied to green bodies. This approach typically involves binder burnout at temperature T_1, followed by short-term heating at temperature T_2 and long-term holding at temperature T_3. All of these steps are carried out within a single thermal cycle. T_2 in two-step sintering process is usually higher than temperature T_3 by no more than several hundred degrees [14]. Preservation of grain size is implied by a densification mechanism in which the diffusion of atoms occurs through stationary grain boundaries [15]. In contrast to the densification of the microstructure through normal grain growth, where grain boundary movement is dominant, ceramics obtained by two-step sintering exhibit a narrow grain size distribution and a small average grain size. This approach leads to excellent results using nano-sized particles as initial powders. However, in most cases, synthesis of nanoparticles with the desired quality is a complex task and significantly increases the overall cost of ceramic production. In this regard, new research on the application of the two-step sintering approach is needed for conventional ceramic technology, which involves the use of industrially produced powders, such as oxides. To ensure a narrow distribution of the initial powders for pressureless two-step sintering, an efficient high-energy milling method can be used [16]. Two-step sintering is essential for the successful synthesis of refractory materials from powder compacts, as the increased proportion of surface atoms in submicron particles enhances atomic diffusion, promoting particle bonding and densification at lower temperatures.

A good model material for conducting studies on the use of two-step annealing is samarium zirconate $Sm_2Zr_2O_7$. Since the end of the 20th century, rare earth zirconates have been considered as a refractory and inert material for structural, functional ceramics, thermal barrier layers and refractories [17,18]. In addition, zirconates $Ln_2Zr_2O_7$ (Ln – lanthanides) are used as oxides for solid oxide fuel cells with high ionic conductivity [19,20], corrosion-resistant refractories [21], materials for storing waste with high radiation activity, as well as materials for dispersed nuclear fuel [22]. $Ln_2Zr_2O_7$ crystallizes in two types of crystal structure – defective fluorite and pyrochlore. The high melting temperatures of ~2300–2500 °C make the sintering of bulk ceramics particularly challenging, as achieving high densification typically requires holding temperatures in the range of 60–70 % of the material's melting point.

Two-step sintering is particularly well-suited for $Sm_2Zr_2O_7$ ceramics. This method enables sufficient densification at reduced sintering temperatures, helping to avoid the exaggerated grain growth typically observed at higher temperatures. Two-step sintering promotes a finer, more uniform microstructure, while preserving the desired crystal phase. Additionally, it reduces energy consumption and minimizes thermal stresses during processing.

To ensure that the experimental conditions closely resemble real manufacturing processes, it is important to use commercially available oxides. While two-step sintering has shown promise in enhancing densification and microstructural control, its application to such industrial-grade powders remains largely unexplored, highlighting the need to study its effectiveness under practical processing conditions. In this study, a micron-sized mixture of Sm_2O_3 and ZrO_2 was used to prepare the green powder. The effects of high-energy mechanical milling and two-step sintering on the resulting properties of $Sm_2Zr_2O_7$ ceramics were systematically investigated.

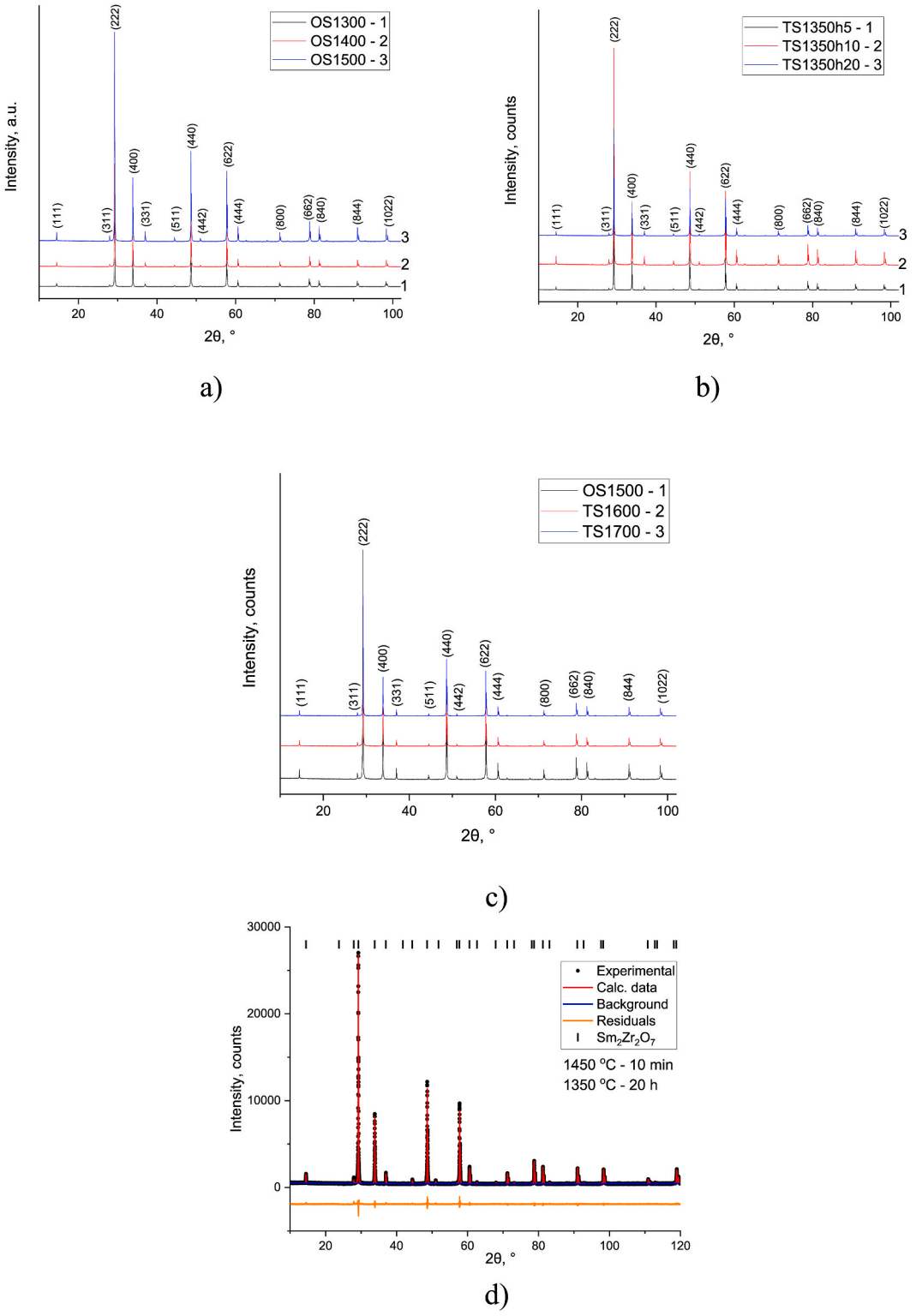

Fig. 2. The XRD patterns of OS (a) and TS (b, c) sample and example of WPPF analysis (d).

2. Experimental

Experimental samples were synthesized by a two-step solid-state sintering process with the assistance of a long-time milling process. All stages of synthesis are represented in Fig. 1. Zirconium oxide ZrO_2 (Sigma Aldrich, Burlington, MA, USA, CAS Registry number 1314-23-4, particle size <5 μm, density 5.89 g/cm^3, purity 99.99 %) and samarium oxide Sm_2O_3 (Sigma Aldrich, Burlington, MA, USA, CAS Registry number 12060-58-1, particle size <5 μm, density 8.35 g/cm^3, purity 99.9 %) were used as starting materials. To obtain the green powder, ZrO_2 and Sm_2O_3 were weighed according to the chemical reaction $2{\bullet}ZrO_2 + Sm_2O_3 \rightarrow Sm_2Zr_2O_7$ (Step I). Homogenization was performed in a planetary mill, Pulversitte 6, 250 rpm, 30 min in a tungsten carbide jar and balls with the addition of ethyl alcohol (Step II). Homogenized powders were annealed at temperatures of 1400 °C for 5 h (Step III). After powder was annealed at 1400 °C, brief X-ray phase analysis

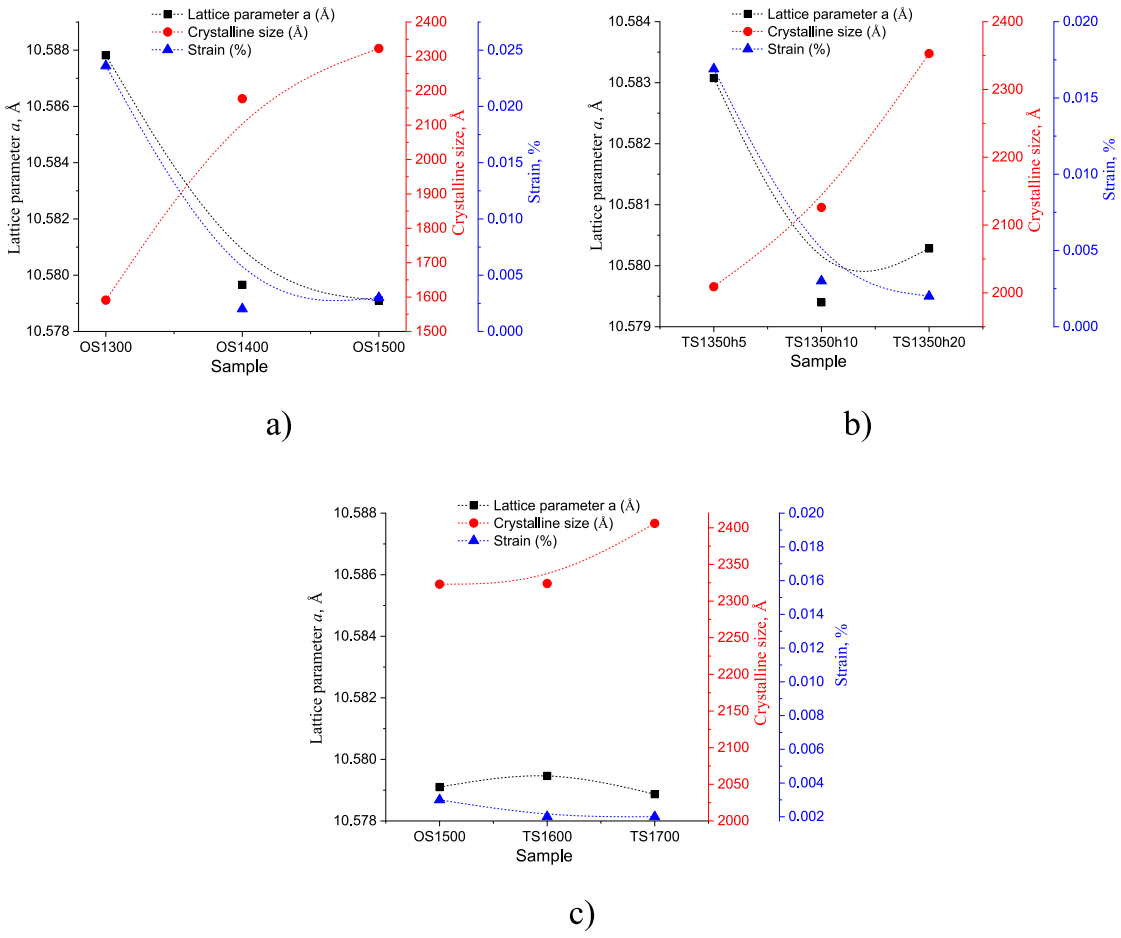

Fig. 3. The comparison of lattice parameters, crystalline size and strain of OS (a) and TS (b, c) samples.

showed formation of the pyrochlore phase $Sm_2Zr_2O_7$. The annealed powder was ground in a Pulverisette 7 planetary mill in a zirconium oxide balls and jar at 500 rpm for 8 h (Step IV). Then, the green powder was produced by mixing a PVA/water solution with grinded powder and sequential evaporation of water in suspension. The resulting press powder was pressed into tablets with a thickness of about 1.2 mm and a diameter of 12 mm (applied pressure 400 MPa, Step V). Then, two-step sintering was performed according to Fig. 1 in a programming Nabertherm LHT 08/18 furnace (Step VI). Temperature regimes, which were used in the programs of sintering, are listed in Table 1.

To study crystal structure parameters and phase composition of obtained samples, the X-ray diffraction (XRD) technique was implemented on the Rigaku SmartLab diffractometer. CuKα source and speed of 2°/min were used to record XRD patterns. XRD patterns were analyzed with the help of the Powder XRD Plugin (Rigaku SmartLab software) using the Whole Powder Pattern Fitting (WPPF) based on the Fundamental Parameters (FP) approach [23,24]. To confirm the identified crystal structure, Raman spectroscopy was implemented. The Raman microscope EnSpectr with a laser wavelength of 532 nm was used to record spectra at room temperatures. For morphology investigations of grains and grain size distribution, optical microscopy and scanning electron microscopy were used together. Optical images of unpolished samples were obtained on the Olympus metallographic microscope. When grains were too small to be detected by optical microscopy, Au-coated tablets were introduced in the electron microscope Thermo Fisher Phenom. Microhardness tests were done by using the Vickers method on the Metkon machine with a load in the range of 10–1000 gf. Before the indentation test samples were polished with the use of diamond paste.

By the analysis of indentation image fracture toughness, estimates were made with the help of the formula [25,26].

$$K_c = 0.0782\left(H_v a^{\frac{1}{2}}\right)\cdot\left(\frac{E}{H_v}\right)^{2/5}(c/a)^{-1.56}, \quad (1)$$

where H_v – Vickers hardness in GPa.

a – half of indentation length,
c – length of crack,
E – Young's modulus.

The values of Young's modulus were measured on the polished surfaces using the Nanoindentation system SMT 5000. To study macroscopic mechanical properties, the Walter Bai universal testing machine was applied with a special custom fixture for the biaxial flexural strength measurements. Flexural strength was estimated using the formula [27].

$$\sigma_t = \frac{3(1+\nu)P}{4\pi t^2}\left[1 + 2\ln\frac{a_c}{b} + \frac{(1-\nu)}{(2+\nu)}\left(1 - \frac{b^2}{2a_c{}^2}\right)\frac{a_c{}^2}{R^2}\right], \quad (2)$$

where σ_t – biaxial flexural strength.

P – crush load in N,
υ – Poisson's ratio (0,3),
t – thickness of tablet,
a_c – radius of the circle on which the spherical supports are located,
b – radius of the pin,

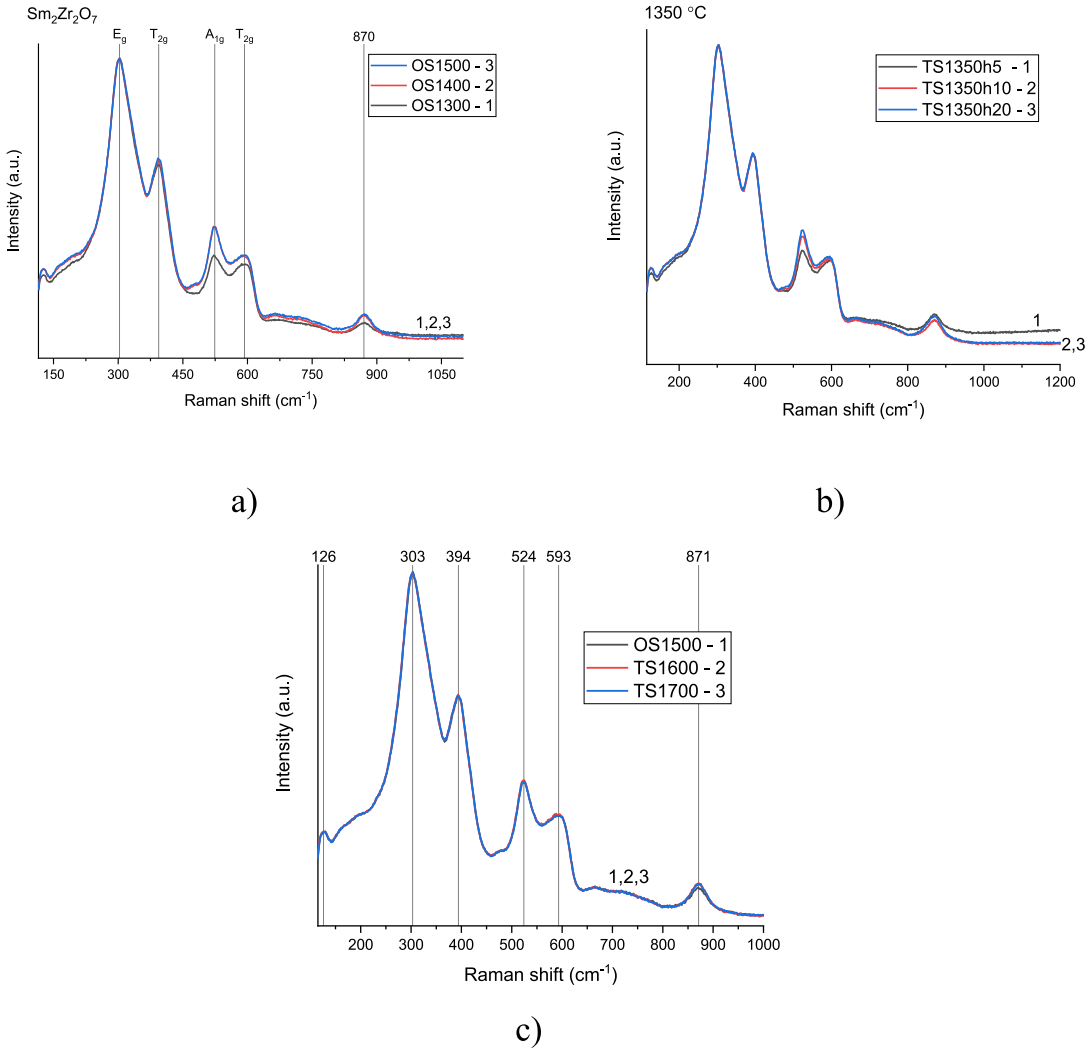

Fig. 4. Raman spectra of ceramic $Sm_2Zr_2O_7$ samples with different sintering regime: OS (a) and TS (b, c).

R – radius of ceramic tablet.

The frequency spectra at room temperature of the dielectric properties were recorded using the RLC meter HIOKI IM3533-01 (Hioki E.E Corporation, Singapore). To estimate permittivity values, a flat capacitor structure was created on every sample by applying an Ag-paste electrode on both sides of the tablets [28].

3. Results and discussion

In Fig. 2, XRD patterns of final experimental samples are shown. It can be seen that all samples are single-phase without any impurities. The crystal structure of synthesized samples is pyrochlore (Fd-3m) due to of the existence of (111), (311), (331), and (511) reflexes in the XRD pattern, PDF 2024-2 Card № 01-075-8266 [29,30]. It can be concluded that after two stages of thermal treatment (pre-annealing and final sintering), all phase transformations are done, and the reaction $Sm_2O_3 + ZrO_2 \rightarrow Sm_2Zr_2O_7$ is completed. However, WPPF analysis revealed that there are some differences in crystal structure, which vary from sintering temperature. The example of WPPF Rietveld analysis is provided in Fig. 2d. It was observed that increasing of sintering temperature for one step sintering samples leads to decreasing of values of lattice parameter *a* from 10.5878 to 10.5791 Å and microstrain from 0.0236 to 0.002 % (Fig. 3a). The explanation of these results is that after high-energy milling, annealed powder exhibits a defect crystal structure with increased lattice parameters and microstrain. This can be seen in the diffraction patterns before and after milling (see Fig. S1a in the supplementary information). After sintering of green compact relaxation processes in crystal structure of powders occurs. Then, the concentration of defects become lower with elimination of mechanical stresses and increasing the value of crystalline size. Latter is significant to the crystallinity of the structure, so it can be concluded that higher temperatures of sintering improve the crystal structure of $Sm_2Zr_2O_7$ bulk ceramics. The same results are provided in another papers where oxide ceramics were studied [31–33]. The similar tendencies for crystallographic parameters were observed for samples obtained by a two-step sintering process with long sintering times TS1350h5, TS1350h10, and TS1350h20 (Fig. 3b). For a variant of two-step sintering with high temperatures (samples TS1600, TS1700, Fig. 3c), changes in crystallographic parameters are less pronounced because of small deviations between maximum and minimum values of *a*, strain, and crystalline size. Change in tendency of these parameters with sintering temperature can be associated with intense recrystallization processes at high temperatures [34]. It can be seen that for samples with a sintering temperature of 1500°C and 1350 °C with a sintering time of more than 5 h, a stress-free crystal structure is detected.

It should be noted that without long-time high-energy milling, ceramic with a sintering regime of 1500 °C – 5h sintered ceramic

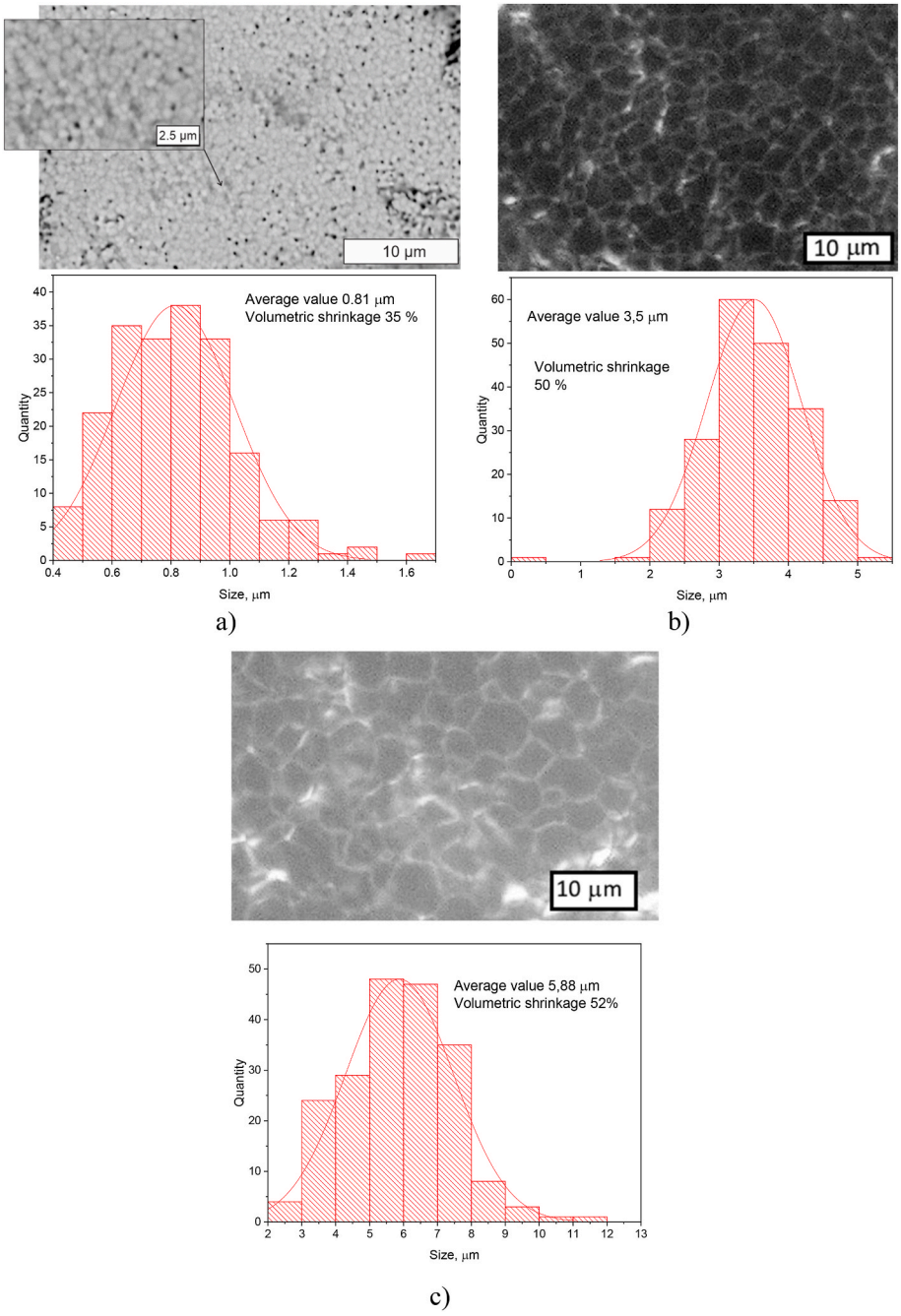

Fig. 5. Surface morphology of ceramics with one sintering step sintering and grain size distribution at different sintering temperatures for samples a) – OS 1300, b) – OS 1400, c) – OS 1500.

changed crystal structure into disordered fluorite Fm-3m, PDF 2024-2 Card N° 01-078-1291 (see the Supplementary Fig. S1b). This result was unexpected, as the intended pyrochlore structure was not formed under these conditions. A plausible explanation for this phase transition is the insufficient homogeneity of the initial Sm_2O_3–ZrO_2 powder mixture due to insufficient duration of milling. Without effective mechanical activation, the diffusion and solid-state reaction between the components during sintering appear to be incomplete, favoring the formation of a defect fluorite phase. This finding highlights the critical role of intensive milling in achieving both phase purity and sufficient densification of ceramics. It also emphasizes that structural control during sintering strongly depends on the quality of powder preparation. Given the complexity and unexpected nature of this structural transition, a detailed investigation into its underlying mechanisms is beyond the scope of the present work. Therefore, in the following sections, the study focuses on samples with confirmed pyrochlore structures obtained through high-energy milling and optimized processing conditions.

Fig. 4 shows the Raman spectra of the $Sm_2Zr_2O_7$ ceramic samples. All spectra contain 5 peaks characteristic of the pyrochlore phase of $Sm_2Zr_2O_7$, while the spectra differ slightly from each other. The peak at 303 cm^{-1} belongs to the E_g mode, which arises from the bending vibrations of O-Sm-O. The peak at 394 cm^{-1} is associated with the T_{2g} mode and stretching vibrations of Zr–O. The peak at 524 cm^{-1} can be attributed to the A_{1g} mode associated with stretching vibrations of Sm–O, and the peak at 593 cm^{-1} to the T_{2g} mode, characterized by stretching vibrations of Sm–O [35]. The peak at 870 cm^{-1} may be related to the T_{2g} mode, which is affected by the distortion of the ZrO_6 octahedron [36]. The small peak in the region of 125 cm^{-1} is not

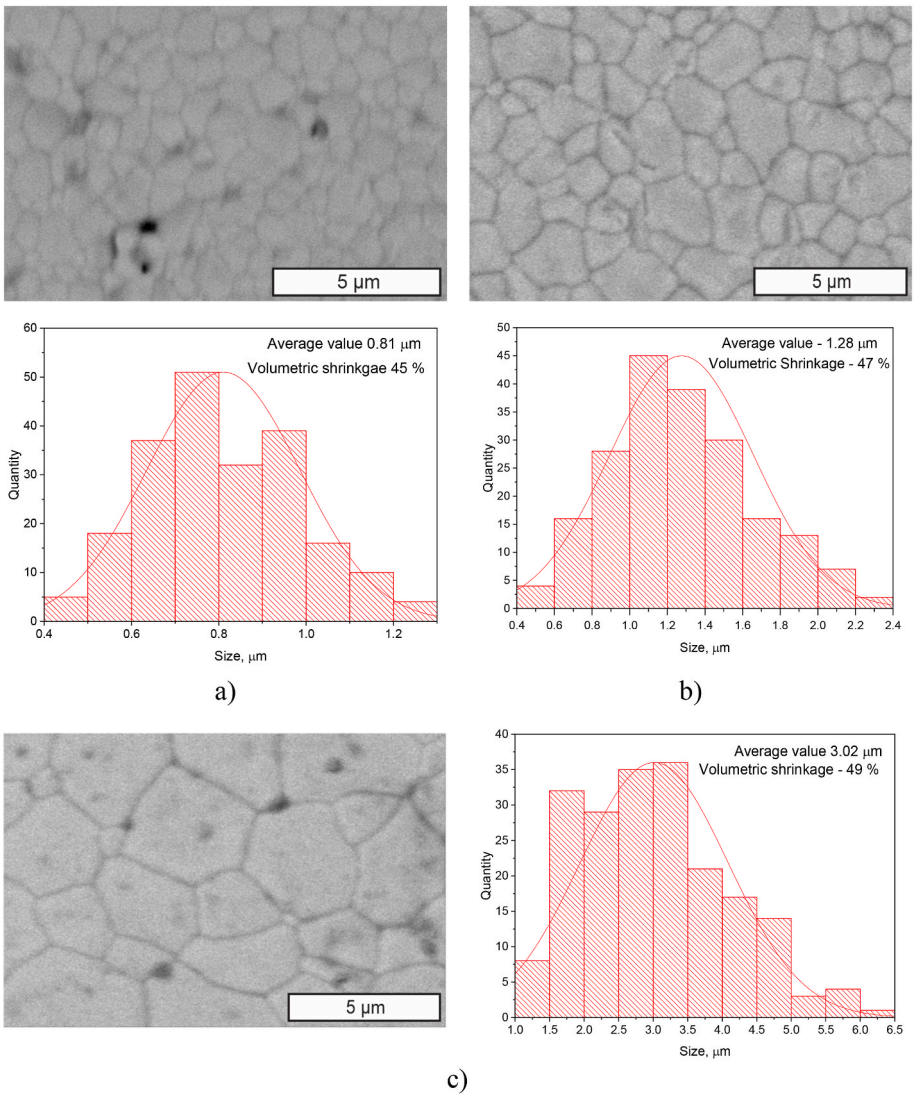

Fig. 6. Surface morphology of ceramics with two sintering steps and grain size distribution at holding temperature 1350 °C for samples a) – TS1350h5, b) – TS1350h10, c) – TS1350h20.

associated with the fundamental vibrational modes in the material, it may relate to anharmonic effects or defects in the material [37].

SEM images of the surface of the experimental samples with grain size distribution are shown in Figs. 5–7. For the sample OS1300 morphology with round grains with an average size of 0.81 μm and intergranular porosity were observed. At such low sintering temperatures, the intensity of the sintering process is limited, and grain boundary migration has not yet occurred. At 1400 °C this energy barrier was overcome, resulting in an increase in average grain size from 0.81 to 3.5 μm and a transition to a polygonal grain morphology. With further increases in sintering temperature, there is sequential growth of the mean size of the grain, accompanied by the emergence of abnormally large grains. This is due to the exaggerated grain growth at high temperatures [38]. Another important indicator of the extensive sintering process is estimated volumetric shrinkage, which increased from 35 % to 50 % when the sintering temperature was changed from 1300 to 1400 °C.

The sintering results for ceramics subjected to a single annealing step showed that only at 1300 °C did the mean grain size remain within the submicron range (prior to annealing, the mean particle size was 0.27 μm as measured by SEM and 0.51 μm according to Analysette 22; see Supplementary Information, Fig. S2 and S3). For this reason, the holding temperature was chosen as 1350 °C in accordance with general suggestions in Ref. [39]. These results showed that high-energy milling and pre-annealing of Sm_2O_3 and ZrO_2 oxides lead to the formation of dense $Sm_2Zr_2O_7$ ceramics at relatively low temperatures.

In the case of two-step sintering with a holding temperature of 1350 °C significant change in surface morphology compared to OS1300 was observed. Polygonal conjuncted grains with a small concentration of intergranular pores and a mean size of grains of 0.81 μm are the main features that occurred after increasing sintering temperature and applying 10 min at 1450 °C (Fig. 6a). However, it was revealed that fraction of several micron-sized grains also increased. For higher holding time (Fig. 6b and c), intergranular pores disappeared, and mean grain size was increased three times compared to holding time of 5h. Unfortunately, the raise of holding time does not lead to the preservation of fine-grain microstructure with decreased porosity. Nevertheless, prolonged sintering at 1350 °C did not result in exaggerated grain growth, in contrast to what was observed at higher sintering temperatures. This conclusion is supported by the lower volumetric shrinkage of the samples sintered at 1350 °C compared to 1500 °C. Although abnormally large grains were not present in the samples, sintered at 1350 °C, extending the annealing time to 10 and 20 hours led to a noticeable increase in average grain size. The primary factor contributing to this increase is the grain boundary movement during sintering [40,41]. To control grain growth under these conditions, the use of grain growth

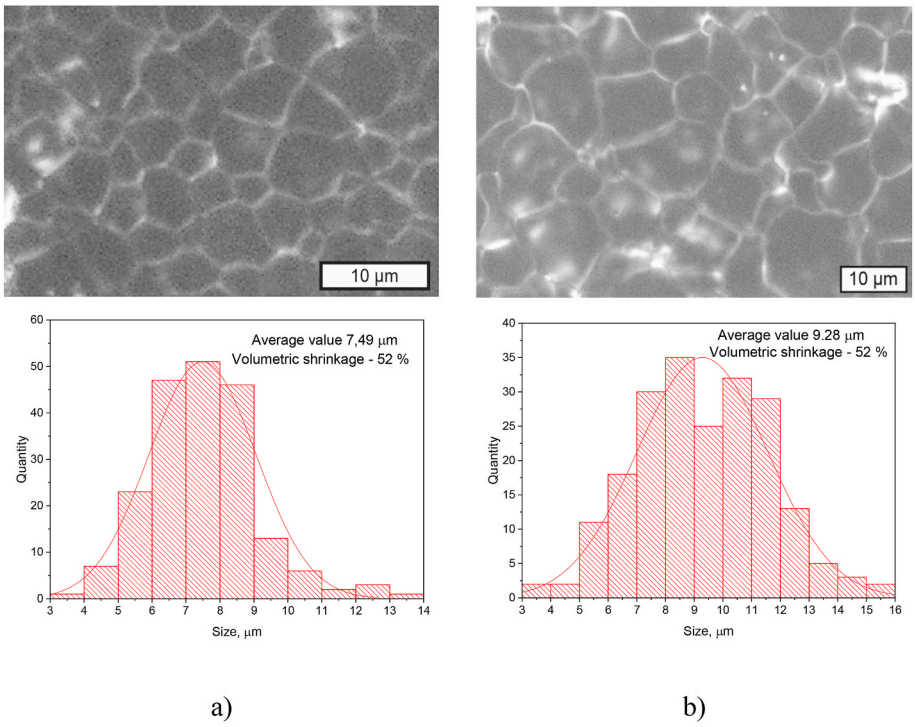

Fig. 7. Surface morphology of ceramics with two sintering steps at holding temperature 1500 °C for samples a) – TS1600, b) – TS1700.

Table 2
Elemental composition in synthesized ceramics estimated by EDX method.

№	Designation	O, at. %	Zr, at. %	Sm, at. %
1	OS1300	65.84	20.28	13.89
2	OS1400	66.44	19.52	14.05
3	OS1500	68.14	17.86	14.00
4	TS1350h5	67.99	19.43	12.59
5	TS1350h10	68.62	18.15	13.23
6	TS1350h20	67.97	19.05	12.98
7	TS1600	68.18	17.00	14.82
8	TS1700	68.00	17.31	14.69

inhibitors may be considered, and adjustments to the sintering temperature profile should be explored.

Two-step sintering with high-temperature steps of 1600 and 1700 °C significantly improves density of ceramics and enlarges the mean grain size to 9.28 μm (Fig. 7). Exaggerated grain growth was observed by detecting large grains with 15–16 μm in size. It is evident that the critical energy of grain boundary movement was exceeded, which in turn leads to an extensive sintering process with pore elimination [42]. As a result, dense ceramics with a wide range of grain sizes were synthesized by applying a two-step sintering process at a holding time of 1500 °C.

According to the chemical formula of $Sm_2Zr_2O_7$ theoretical ratio of Sm:Zr:O should be 18:18:64 %. Elemental compositions of all samples are provided in Table 2. It can be seen that there is an excess of oxygen and zirconium, which can be explained as follows. During SEM investigations, dielectric $Sm_2Zr_2O_7$ ceramics were covered by 15 nm of gold to avoid charging of surface. On the EDX spectra, the Zr and Au elements Au-M and Zr–K lines are overlapped, which brings uncertainty in the estimated composition (see Fig. S4 in supplementary). Nevertheless, obtained values of atomic percentages are close to theoretical, which confirms the formation of pyrochlore samarium zirconate.

HV microhardness comparison of the obtained ceramics is presented in Fig. 8. Microhardness measurements were carried out at various loads to study the hardness under the influence of various deformation mechanisms that occur during indentation. It can be said that for samples with low sintering temperatures, characterized by increased porosity, the microhardness values are lower by 400–600 HV than in samples with high sintering temperatures and long holding. Also, for these samples, a decrease in microhardness values with increasing load is observed. Such results can be explained by the fact that at high loads (area of pure plastic deformations) a larger volume of material and, consequently, a larger number of pores begin to participate in compression resistance. Since pores are concentrators of dislocations, the destruction of the material on them occurs at lower stresses [43]. An interesting result can be highlighted for the TS1350h10 sample, which shows a maximum microhardness of 1400 at low load values. This can be explained by the small average grain size of 1.28 μm among all samples and low porosity. It is known that a decrease in grain size leads to strengthening of ceramics due to the hindered propagation of cracks at grain boundaries, the number of which increases with decreasing grain size [44]. Thus, under elastic-plastic deformations, the resistance to indentation of ceramics with a smaller grain size increases. For high sintering temperatures and sample TS1350h20, an HV value of about 1200 is observed, which weakly depends on the indentation load. This indicates that for this sample, no different deformation mechanisms are observed during indentation and that the sample has low porosity.

Fig. 9 shows the results of calculations of the biaxial bending strength for the all samples under study. This parameter, unlike microhardness, shows the mechanical properties of the bulk material at the macro level. It can be seen that an increase in the sintering temperature (Fig. 9a) leads to a significant increase in the bending strength from 46 to 83 MPa, which can be explained by an increase in the shrinkage value and a decrease in porosity. With two-step sintering for samples TS1350h5, TS1350h10, TS1350h20, the holding time also leads to a pronounced increase in strength from 66 to 123 MPa. An interesting fact is revealed when analyzing the effect of two-step sintering with a holding temperature of 1500 °C on the biaxial bending strength. From Fig. 9c it can be seen that the use of two-step sintering at a temperature of 1700 °C for 10 min also leads to an increase in the biaxial flexural strength from 83 to 125 MPa, as in sample TS1350h20. It can be stated that both types of two-step sintering lead to similar final values of the mechanical properties. When comparing the results of the study of the crystal structure

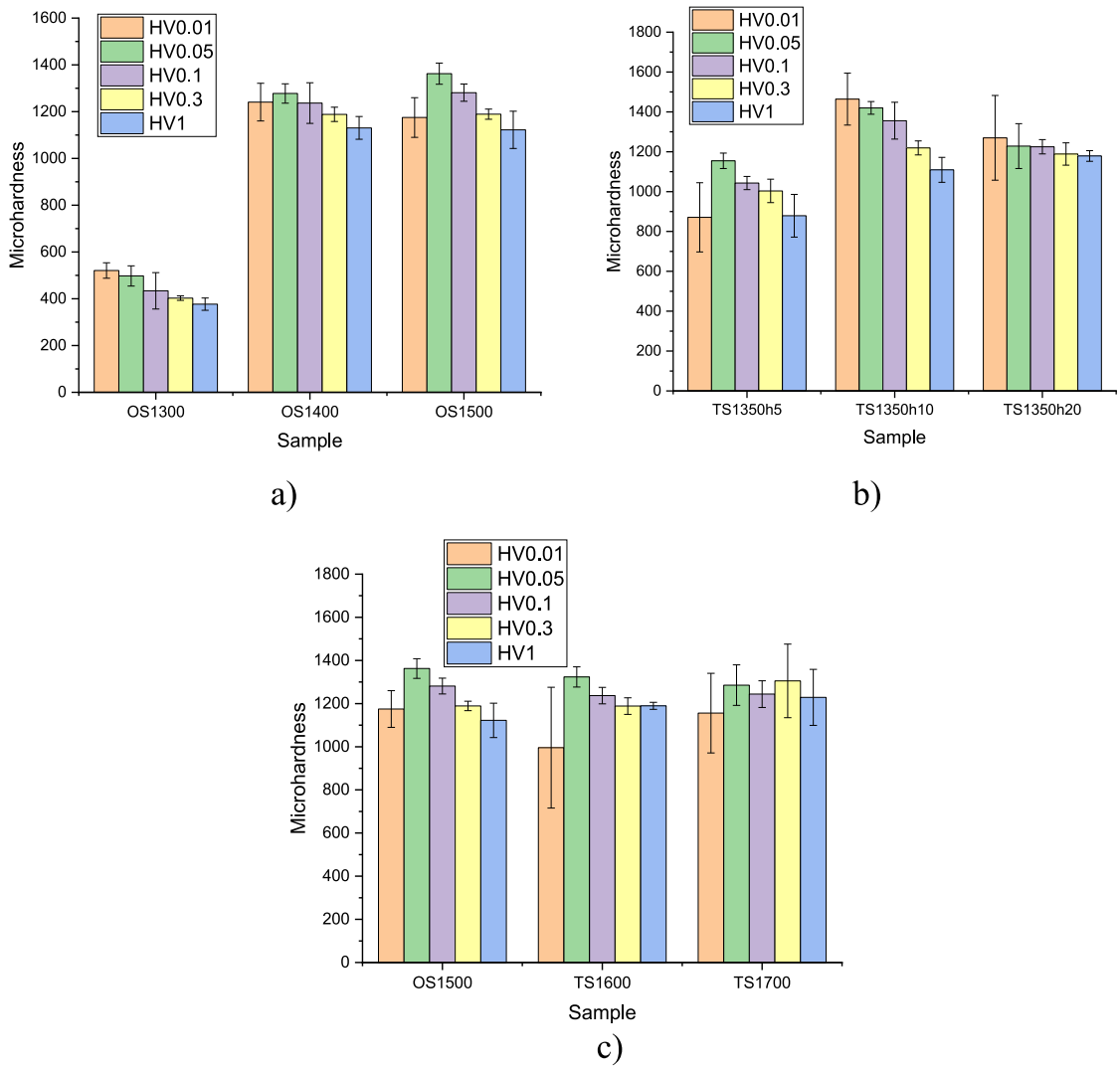

Fig. 8. Comparison of Vickers microhardness for samples with one sintering step (a) and two sintering steps (b, c).

and mechanical tests, it can be assumed that the improvement of the mechanical properties is associated with the reduction of internal stresses. This stress relaxation becomes more pronounced either with an increase in the temperature of the first sintering strep or with prolonged holding time during the second step. XRD analysis confirms that these conditions promote the formation of a more relaxed and uniform crystal structure. A relaxed crystal structure helps prevent local stress concentrations that could otherwise promote defect formation and contribute to mechanical degradation under applied loads. At the same time, the microstructure of ceramics with the best mechanical properties is noticeably different: sample 1350h20 has a smaller average grain size and a narrower size distribution compared to sample TS1700.

The frequency dependences of the permittivity and loss tangent measured at room temperature are shown in Figs. 10 and 11, respectively. The permittivity ε' is a structure-sensitive parameter that shows the ability of the material to polarize in an electric field. The obtained samples are characterized by lower permittivity values of 18–31 in comparison with other zirconates and solid solutions, where they act as one of the components [45–47]. This is due to the fact that the dipole moments in the cubic structure of pyrochlore are less significant than in tetragonal structures in oxygen polyhedra of titanates or solid solutions of titanates-zirconates. Figs. 10a and b clearly show that increasing the sintering temperature and holding time leads to a higher permittivity. Such changes directly correlate with the growth of the grain size and the values of volume shrinkage. Along with this, porosity can significantly reduce the value of the permittivity and the presence of high porosity in the samples OS1300, TS1350h5 causes the minimum values of ε'. In a polycrystal with large grains, the induction of the electric field is more uniform, since the proportion of the surface of grain boundaries, which can have other dielectric properties compared to the grains, decreases. It is believed that in crystals with a uniform structure, the value of the permittivity is higher, since there is a higher intensity of the polarization process [48,49]. It can be noted that the frequency dependences ε'(f) do not have a pronounced dispersion, which may indicate the absence of the influence of grain boundaries on low-frequency dielectric characteristics [28]. The highest value of dielectric constant at a frequency of 500 Hz is found in the 1700 °C sample, which can be associated with the largest average grain size in the microstructure of the sample.

Dielectric losses expressed through the tangent of the dielectric loss angle tan δ are shown in Fig. 11. As can be seen from the figure, dielectric losses, as well as ε', are not characterized by significant changes with increasing frequency and have values in the range of 0.01–0.025 for all samples. Moreover, the range of loss tangent values does not allow us to characterize the obtained $Sm_2Zr_2O_7$ ceramics as a high-quality dielectric. There are a large number of factors affecting dielectric losses in polycrystals: grain size, porosity, heterogeneity in chemical composition in grains and intergranular boundaries, impurities, defects in crystallites [50]. The reason for the relatively high

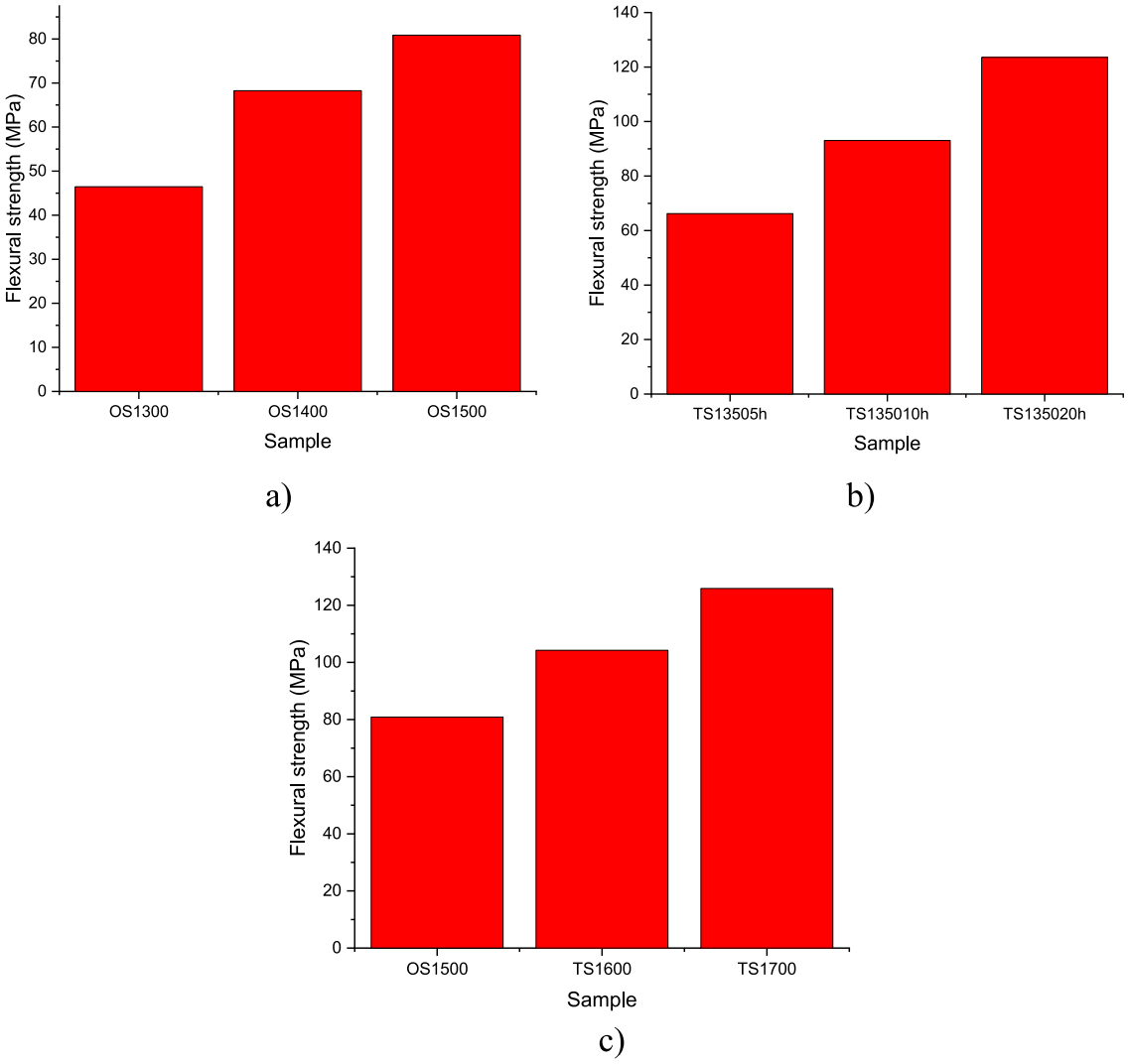

Fig. 9. Comparison of biaxial flexural strength for one-step sintered (a) and two-step sintered (b, c) specimens.

values of dielectric losses in the $Sm_2Zr_2O_7$ polycrystal may be the nature of the crystal itself. The pyrochlore structure is close to the fluorite structure, but it contains oxygen vacancies that can lead to the emergence of polarons and polaron conductivity. Also, the crystal lattice may have antistructural defects that lead to the emergence of polaron conductivity. The contribution from such conductivity may exceed the dielectric losses due to interaction with phonons. As a result, the losses in $Sm_2Zr_2O_7$ within the frequency range of 500 Hz to 200 kHz can be several orders of magnitude higher than those observed in other oxide ceramic polycrystals [51].

As a final graph of this study, a comparison of crack resistance, grain size and porosity for all the samples produced should be given (Fig. 12). It is known that for many materials the dependence of strength on crack resistance is linear [52]. Fracture in crystals with ionic bonds is associated with the propagation of dislocations and cracks; therefore, the K_i parameter should be considered as the main indicator characterizing the mechanical properties of the synthesized ceramics [53]. As can be seen from Fig. 12, for samples with high porosity and small average grain size (less than 1 μm), the crack resistance K_i value is 0.8–1 MPa·m$^{1/2}$. Despite the fine-grained structure, the mechanical characteristics of these ceramics are significantly worse in comparison with other ceramics of this work. In the case of samples OS1300, TS1350h5, the mechanical properties were determined to a greater extent by porosity. With an increase in the holding time during two-step sintering at a temperature of 1350 °C, the crack resistance increased to 1.3 MPa·m$^{1/2}$, which is higher than that of sample OS1500. The porosity of samples OS1500 and TS1350h20 was 6 and 8 %, and the average grain size was 5.88 and 3.02 μm, respectively. Although this comparison may indicate a significant influence of the microstructure on the mechanical properties, the TS1700 sample violates this assumption. The increase in fracture toughness in samples with the same porosity can be associated with an increase in the crystallite size, which was established by X-ray diffraction analysis (Fig. 3c). The best fracture toughness of 1.6 MPa·m$^{1/2}$ and the highest value of biaxial bending strength are characterized by the TS1700 sample. Moreover, the uncontrolled grain growth observed in this sample after analysis of the microstructure. For this reason, the following conclusion can be made for samarium zirconate ceramics sintered using standard ceramic technology without high pressure. Crack propagation and, consequently, fracture toughness depend to a greater extent on the porosity of $Sm_2Zr_2O_7$ ceramics than on the average grain size.

4. Conclusions

The effect of high-energy mechanical milling and two-step sintering technique on the properties of $Sm_2Zr_2O_7$ bulk ceramics was investigated. It has been experimentally established that in the case of using submicron powders of the Sm_2O_3+ZrO_2 mixture, which were pre-annealed

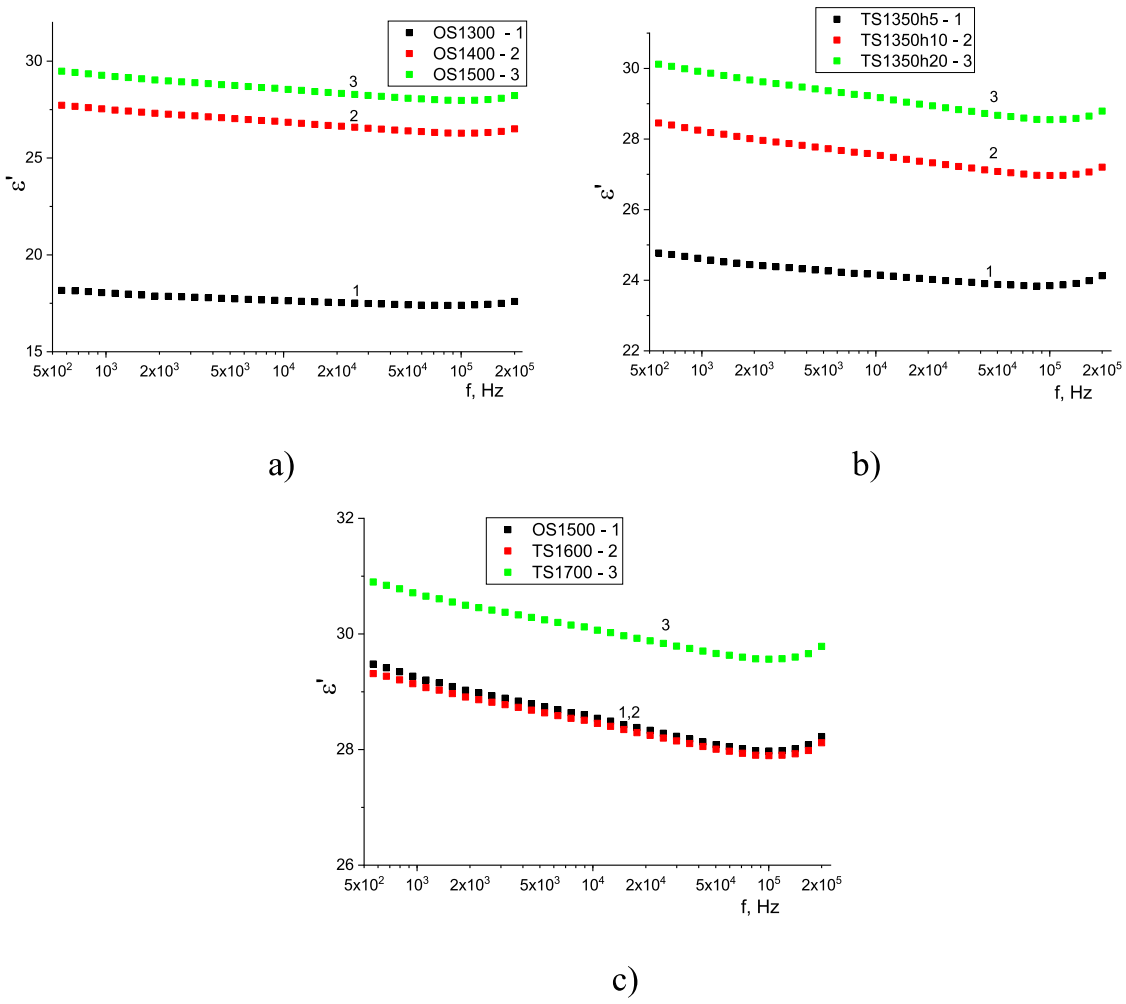

Fig. 10. Frequency dependence of permittivity of one-step sintered (a) and two-step sintered (b, c) specimens.

and ground at 500 rpm and 8 h, it is possible to obtain a single-phase polycrystalline material already at a sintering temperature of 1300 °C. It was found that two types of two-step sintering (at high temperatures and long holding time) make it possible to obtain ceramics with high value of microhardness, biaxial bending strength and crack resistance. Analysis of the results of X-ray structural analysis and scanning electron microscopy methods made it possible to determine that the change in the mechanical characteristics of the synthesized ceramics is mainly determined by the porosity of the sintered bodies, and not by the average grain size or grain size distribution. The dielectric characteristics of the obtained samples, as shown by the analysis of the microstructure and dielectric spectroscopy, are determined by both the porosity and the average grain size. The conducted study revealed that synthesizing $Sm_2Zr_2O_7$ ceramics from submicron powders under conditions close to real manufacturing does not lead to the significant improvement in mechanical characteristics through two-step sintering. This improvement is typically expected from the preservation of a fine-grained and homogeneous structure, which appears to be difficult to achieve under these conditions. For this reason, the use of standard approaches to pressureless sintering of $Sm_2Zr_2O_7$ is recommended, which guarantees excellent mechanical properties of the material.

CRediT authorship contribution statement

I.E. Kenzhina: Supervision, Conceptualization, Writing – review & editing, Funding acquisition. **A.L. Kozlovskiy:** Supervision, Conceptualization, Writing – review & editing, Methodology. **R.I. Shakirzyanov:** Writing – original draft, Methodology, Conceptualization, Writing – review & editing, Visualization, Formal analysis. **M.E. Kaliyekperov:** Methodology, Data curation, Visualization, Investigation. **N.O. Volodina:** Visualization, Data curation, Writing – review & editing, Methodology. **S.A. Maznykh:** Visualization, Investigation, Methodology. **M. Begentayev:** Visualization, Investigation, Methodology, Formal analysis. **S.K. Askerbekov:** Formal analysis, Writing – review & editing, Conceptualization. **Zh.A. Zaurbekova:** Writing – review & editing, Data curation, Supervision. **A.U. Tolenova:** Visualization, Writing – original draft, Investigation. **P.A. Blynskiy:** Visualization, Data curation, Writing – original draft, Methodology.

Availability of data and materials

Data sets generated during the current study are available from the corresponding author on reasonable request.

Funding

This work was carried out within the framework of program-targeted funding (program No. BR21882237 «Development and research of advanced composite materials for energy and the fuel cycle») with the support of the Science Committee of the Ministry of Science and Higher Education of the Republic of Kazakhstan.

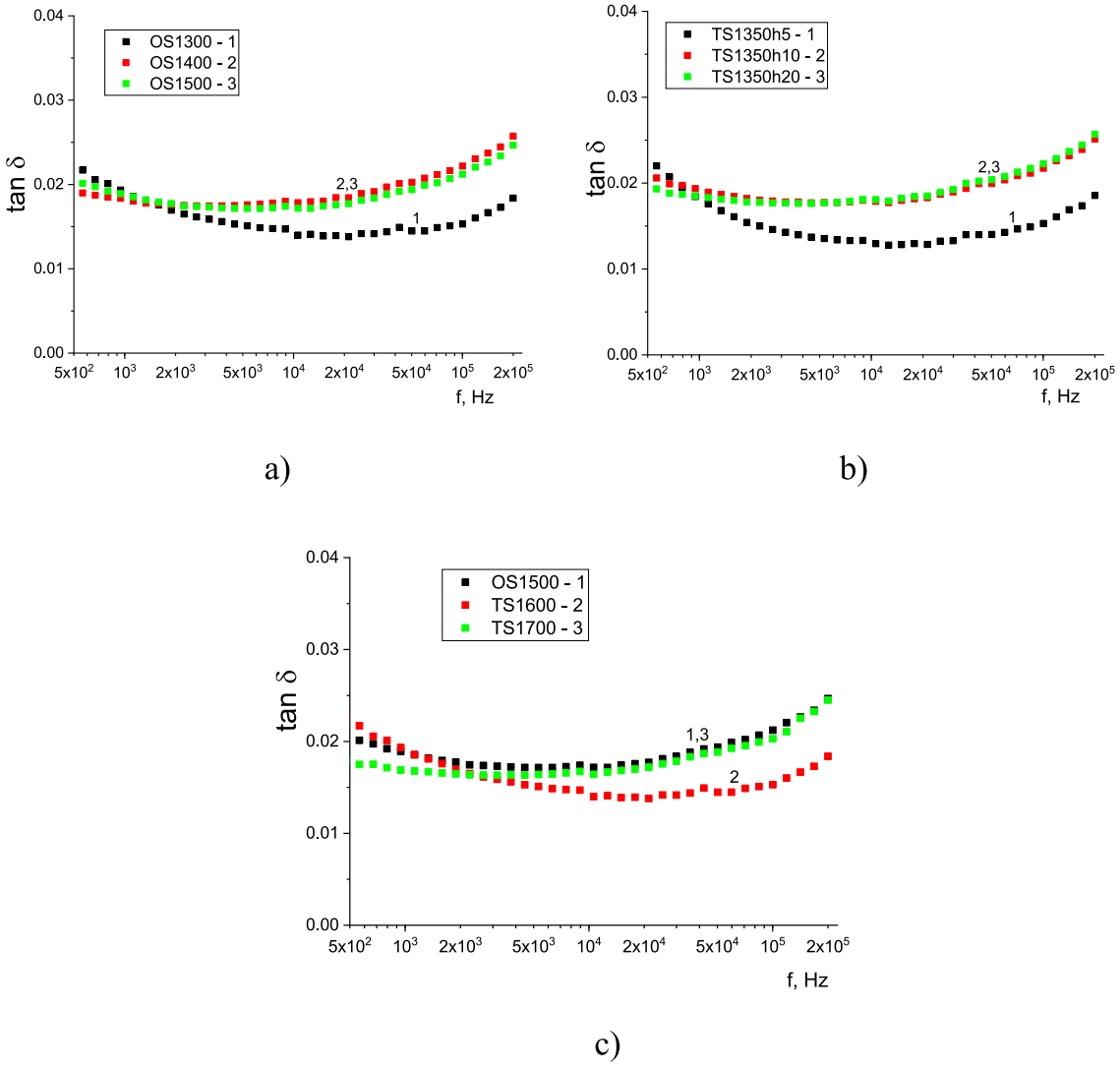

Fig. 11. Frequency dependence of loss tangent of one-step sintered (a) and two-step sintered (b, c) specimens.

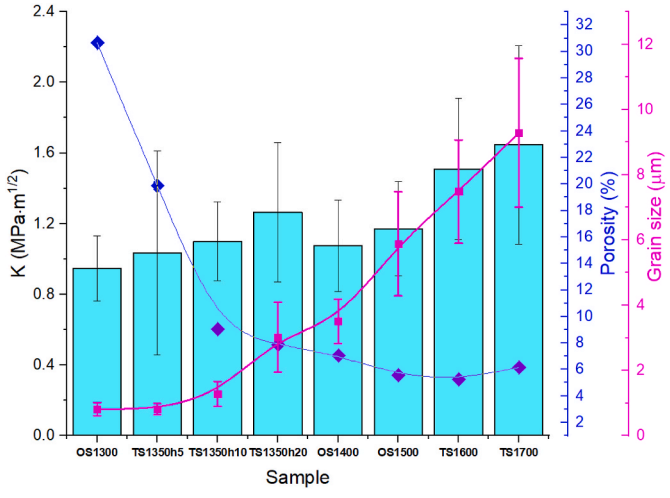

Fig. 12. The comparison of fracture toughness, porosity and mean grain size of all experimental samples.

Declaration of competing interest

The authors declare that they have no known competing financial interests or personal relationships that could have appeared to influence the work reported in this paper.

Appendix A. Supplementary data

Supplementary data to this article can be found online at https://doi.org/10.1016/j.cscee.2025.101270.

Data availability

Data will be made available on request.

References

[1] O. Akhlaghi, E. Camposilvan, Z. Goharibajestani, S.K. Abkenar, C.W. Ow-Yang, Y. Jorand, L. Gremillard, V. Garnier, J. Chevalier, Transparent high-strength nanosized yttria stabilized zirconia obtained by pressure-less sintering, J. Eur. Ceram. Soc. 42 (2022) 7187–7195, https://doi.org/10.1016/J.JEURCERAMSOC.2022.07.027.

[2] D. Hotza, D.E. García, R.H.R. Castro, Obtaining highly dense YSZ nanoceramics by pressureless, unassisted sintering, Int. Mater. Rev. 60 (2015) 353–375, https://doi.org/10.1179/1743280415Y.0000000005.

[3] H. Ryou, J.W. Drazin, K.J. Wahl, S.B. Qadri, E.P. Gorzkowski, B.N. Feigelson, J. A. Wollmershauser, Below the hall-petch limit in nanocrystalline ceramics, ACS Nano 12 (2018) 3083–3094, https://doi.org/10.1021/ACSNANO.7B07380.

[4] J.W. Drazin, J.A. Wollmershauser, H. Ryou, M.A. Wolak, E.P. Gorzkowski, Pressureless low temperature sintering of nanocrystalline zirconia ceramics via dry powder processing, J. Am. Ceram. Soc. 103 (2020) 60–69, https://doi.org/10.1111/JACE.16690.

[5] C. Yang, A. Thron, R.H.R. Castro, Grain boundary strengthening in nanocrystalline zinc aluminate, J. Am. Ceram. Soc. 102 (2019) 6904–6912, https://doi.org/10.1111/JACE.16512.

[6] A.G. Sheinerman, M.Y. Gutkin, The role of grain boundaries and their triple junctions in strengthening and softening of nanocrystalline ceramics, Lett. Mater. 10 (2020) 547–550, https://doi.org/10.22226/2410-3535-2020-4-547-550.

[7] A.Y. Mironovich, V.G. Kostishin, H.I. Al-Khafaji, A.V. Timofeev, E.S. Savchenko, A. I. Ril, Submicron barium hexaferrite ceramics manufactured by low-temperature liquid-phase sintering of $BaFe_{12}O_{19}$ nanoparticles, Russ. J. Inorg. Chem. (2024), https://doi.org/10.1134/S0036023624602630.

[8] M. Tokita, Progress of Spark Plasma Sintering (SPS) method, systems, ceramics applications and industrialization, Ceramics 4 (4) (2021) 160–198, https://doi.org/10.3390/CERAMICS4020014 (2021) 160–198.

[9] M.H. Bocanegra-Bernal, Hot isostatic pressing (HIP) technology and its applications to metals and ceramics, J. Mater. Sci. 39 (2004) 6399–6420, https://doi.org/10.1023/B:JMSC.0000044878.11441.90/METRICS.

[10] S.M. Barinov, V.F. Ponomarev, V.Y. Shevchenko, Effect of hot isostatic pressing on the mechanical properties of aluminum oxide ceramics, Refract. Ind. Ceram. 38 (1997) 9–12, https://doi.org/10.1007/BF02768225/METRICS.

[11] X. Lv, X. Li, J. Huang, C. Ge, Q. Yu, Effect of ultra-high pressure sintering and spark plasma sintering and subsequent heat treatment on the properties of Si3N4 ceramics, Materials 15 (15) (2022) 7309, https://doi.org/10.3390/MA15207309 (2022) 7309.

[12] S. Marinel, C. Manière, A. Bilot, C. Bilot, C. Harnois, G. Riquet, F. Valdivieso, C. Meunier, C. Coureau, F. Barthélemy, Microwave sintering of Alumina at 915 MHz: modeling, process control, and microstructure distribution, Materials 12 (12) (2019) 2544, https://doi.org/10.3390/MA12162544 (2019) 2544.

[13] Y. Garanin, R. Shakirzyanov, D. Borgekov, A. Kozlovskiy, N. Volodina, D. Shlimas, M. Zdorovets, Study of morphology, phase composition, optical properties, and thermal stability of hydrothermal zirconium dioxide synthesized at low temperatures, Sci. Rep. 14 (14) (2024) 1–12, https://doi.org/10.1038/s41598-024-80399-x, 1 (2024).

[14] N.J. Lóh, L. Simão, C.A. Faller, A. De Noni, O.R.K. Montedo, A review of two-step sintering for ceramics, Ceram. Int. 42 (2016) 12556–12572, https://doi.org/10.1016/J.CERAMINT.2016.05.065.

[15] I.W. Chen, X.H. Wang, Sintering dense nanocrystalline ceramics without final-stage grain growth, Nature 404 (404) (2000) 168–171, https://doi.org/10.1038/35004548, 6774 (2000).

[16] D.L. Zhang, Processing of advanced materials using high-energy mechanical milling, Prog. Mater. Sci. 49 (2004) 537–560, https://doi.org/10.1016/S0079-6425(03)00034-3.

[17] J. Wu, X. Wei, N.P. Padture, P.G. Klemens, M. Gell, E. García, P. Miranzo, M. I. Osendi, Low-Thermal-Conductivity rare-earth zirconates for potential thermal-barrier-coating applications, J. Am. Ceram. Soc. 85 (2002) 3031–3035, https://doi.org/10.1111/J.1151-2916.2002.TB00574.X.

[18] M.K. Hossain, M.H.K. Rubel, M.A. Akbar, M.H. Ahmed, N. Haque, M.F. Rahman, J. Hossain, K.M. Hossain, A review on recent applications and future prospects of rare earth oxides in corrosion and thermal barrier coatings, catalysts, tribological, and environmental sectors, Ceram. Int. 48 (2022) 32588–32612, https://doi.org/10.1016/J.CERAMINT.2022.07.220.

[19] R. Zhang, Q. Xu, W. Pan, C.L. Wan, L.H. Qi, H.Z. Miao, Structure and ionic conductivity of Ln2Zr2O7-Type rare Earth zirconates, Key Eng. Mater. 336–338 (2007) 420–423, https://doi.org/10.4028/WWW.SCIENTIFIC.NET/KEM.336-338.420.

[20] C. Yang, T. Zheng, Z. Li, F. Yu, H. Sun, F. Gapsari, J. Sunarso, High-Performance high-entropy perovskite cathodes with A-Site deficiency and Ni doping derived from $La_xSr_{1-x}Co_yFe_{1-y}O_{3-\delta}$ for solid oxide fuel cells, Ceram. Int. 51 (2025) 15837–15845, https://doi.org/10.1016/j.ceramint.2025.01.421.

[21] C. Gui, Z.J. Peng, J.T. Yao, S.Q. Wang, Z.G. Liu, Y.M. Wang, J.H. Ouyang, Improving corrosion resistance of rare Earth zirconates to calcium–magnesium–alumina–silicate molten salt through high-entropy strategy, Materials 17 (2024) 6254, https://doi.org/10.3390/MA17246254.

[22] A.L. Kozlovskiy, M.B. Kabiev, D.I. Shlimas, V.V. Uglov, Study of the effect of the formation of two-phase ceramics based on neodymium zirconate due to doping with mgo and Y_2O_5 on the stability of strength and thermophysical parameters under irradiation, Eurasian Phy. Tech. J. 21 (2024) 5–13, https://doi.org/10.31489/2024NO2/5-13.

[23] H. Toraya, Whole-powder-pattern fitting without reference to a structural model: application to X-ray powder diffraction data, J. Appl. Crystallogr. 19 (1986) 440–447, https://doi.org/10.1107/S0021889886088982.

[24] A. Le Bail, Whole powder pattern decomposition methods and applications: a retrospection, Powder Diffr. 20 (2005) 316–326, https://doi.org/10.1154/1.2135315.

[25] D. Ćorić, L. Ćurković, M.M. Renjo, Statistical analysis of vickers indentation fracture toughness of Y-TZP ceramics, Trans. FAMENA 41 (2017) 1–16, https://doi.org/10.21278/TOF.41201.

[26] C.B. Ponton, R.D. Rawlings, Vickers indentation fracture toughness test Part 1 Review of literature and formulation of standardised indentation toughness equations, Mater. Sci. Technol. 5 (1989) 865–872, https://doi.org/10.1179/MST.1989.5.9.865.

[27] S.M. Chung, A.U.J. Yap, S.P. Chandra, C.T. Lim, Flexural strength of dental composite restoratives: Comparison of biaxial and three-point bending test, J. Biomed. Mater. Res. B Appl. Biomater. 71B (2004) 278–283, https://doi.org/10.1002/JBM.B.30103.

[28] R.I. Shakirzyanov, N.O. Volodina, K.K. Kadyrzhanov, A.L. Kozlovskiy, D.I. Shlimas, G.A. Baimbetova, D.B. Borgekov, M.V. Zdorovets, Study of the aid effect of CuO-TiO_2-Nb_2O_5 on the dielectric and structural properties of Alumina ceramics, Materials 16 (16) (2023) 5018, https://doi.org/10.3390/MA16145018 (2023) 5018.

[29] M.C. Hatnean, C. Decorse, M.R. Lees, O.A. Petrenko, G. Balakrishnan, Zirconate pyrochlore frustrated magnets: crystal growth by the floating Zone technique, Crystals 6 (6) (2016) 79, https://doi.org/10.3390/CRYST6070079 (2016) 79.

[30] M. Ciomaga Hatnean, M.R. Lees, G. Balakrishnan, Growth of single-crystals of rare-earth zirconate pyrochlores, $Ln_2Zr_2O_7$ (with Ln=La, Nd, Sm, and Gd) by the floating zone technique, J. Cryst. Growth 418 (2015) 1–6, https://doi.org/10.1016/J.JCRYSGRO.2015.01.037.

[31] N. Sharma, A.K. Mall, R. Gupta, A. Garg, S. Kumar, Effect of sintering temperature on structure and properties of $GaFeO_3$, J. Alloys Compd. 737 (2018) 646–654, https://doi.org/10.1016/J.JALLCOM.2017.12.122.

[32] M.M. Syazwan, A.N. Hapishah, R.S. Azis, Z. Abbas, M.N. Hamidon, Grain growth effects on magnetic properties of $Ni_{0.6}Zn_{0.4}Fe_2O_4$ material prepared using mechanically alloyed nanoparticles, Results Phys. 9 (2018) 842–850, https://doi.org/10.1016/J.RINP.2018.03.054.

[33] A. Gaur, G.D. Varma, Sintering temperature effect on electrical transport and magnetoresistance of nanophasic $La_{0.7}Sr_{0.3}MnO_3$, J. Phys. Condens. Matter 18 (2006) 8837, https://doi.org/10.1088/0953-8984/18/39/014.

[34] S.G. Oleinik, N.V. Danilenko, Primary recrystallization mechanisms in ceramic materials, Powder Metall. Met Ceram. 37 (1998) 55–66, https://doi.org/10.1007/BF02677231/METRICS.

[35] S. Wu, Z. Xue, X. Ji, E. Byon, S. Zhang, Influence of $Y_3Al_5O_{12}$ doping on mechanical properties and thermal conductivity of $Sm_2Zr_2O_7$-$Y_3Al_5O_{12}$ composite ceramics, J. Alloys Compd. 842 (2020) 155872, https://doi.org/10.1016/J.JALLCOM.2020.155872.

[36] U.A. Renju, P. Prabhakar Rao, Contrasting anion disorder behavior in $Sm_2Zr_2O_7$ by simultaneous aliovalent cation substitutions and its structural and electrical properties, J. Appl. Phys. 126 (2019), https://doi.org/10.1063/1.5100237/157412.

[37] Z. Qu, C. Wan, W. Pan, Thermal expansion and defect chemistry of MgO-doped $Sm_2Zr_2O_7$, Chem. Mater. 19 (2007) 4913–4918, https://doi.org/10.1021/CM071615Z.

[38] Philippe Boch, J.-Claude. Niepce, Ceramic Materials : Processes, Properties, and Applications, 2010, p. 593.

[39] Y. Dong, H. Yang, L. Zhang, X. Li, D. Ding, X. Wang, J. Li, J. Li, I.W. Chen, Ultra-Uniform nanocrystalline materials via two-step sintering, Adv. Funct. Mater. 31 (2021) 2007750, https://doi.org/10.1002/ADFM.202007750.

[40] K. Matsui, H. Yoshida, Y. Ikuhara, Review: microstructure-development mechanism during sintering in polycrystalline zirconia, Int. Mater. Rev. 63 (2018) 375–406, https://doi.org/10.1080/09506608.2017.1402424.

[41] J. Hostaša, F. Picelli, S. Hříbalová, V. Nečina, Sintering aids, their role and behaviour in the production of transparent ceramics, Open Ceramics 7 (2021) 100137, https://doi.org/10.1016/J.OCERAM.2021.100137.

[42] K.R. Kambale, A. Mahajan, S.P. Butee, Effect of grain size on the properties of ceramics, Met. Powder Rep. 74 (2019) 130–136, https://doi.org/10.1016/J.MPRP.2019.04.060/ASSET/IMAGES/LARGE/J.MPRP.2019.04.060_GR1.JPEG.

[43] Q. Tang, J. Gong, Effect of porosity on the microhardness testing of brittle ceramics: a case study on the system of NiO-ZrO_2, Ceram. Int. 39 (2013) 8751–8759, https://doi.org/10.1016/J.CERAMINT.2013.04.061.

[44] P. Palmero, Structural ceramic nanocomposites: a review of properties and powders' synthesis methods, Nanomaterials 5 (5) (2015) 656–696, https://doi.org/10.3390/NANO5020656 (2015) 656–696.

[45] S. Roberts, Dielectric properties of lead zirconate and barium-lead zirconate, J. Am. Ceram. Soc. 33 (1950) 63–66, https://doi.org/10.1111/J.1151-2916.1950.TB14168.X.

[46] J.Q. Qi, B.B. Liu, H.Y. Tian, H. Zou, Z.X. Yue, L.T. Li, Dielectric properties of barium zirconate titanate (BZT) ceramics tailored by different donors for high voltage applications, Solid State Sci. 14 (2012) 1520–1524, https://doi.org/10.1016/J.SOLIDSTATESCIENCES.2012.08.009.

[47] K. Hkiri, M. Ben Salem, A. Othmani, M. Zouaoui, Electrical and dielectric properties study of $CaZrO_3$-$CaTiO_3$ composite system by impedance spectroscopy, Ionics 26 (2020) 5099–5111, https://doi.org/10.1007/S11581-020-03596-4/METRICS.

[48] P. Mao, J. Wang, S. Liu, L. Zhang, Y. Zhao, L. He, Grain size effect on the dielectric and non-ohmic properties of $CaCu_3Ti_4O_{12}$ ceramics prepared by the sol-gel process, J. Alloys Compd. 778 (2019) 625–632, https://doi.org/10.1016/J.JALLCOM.2018.11.200.

[49] T. Li, Z. Chen, Y. Su, L. Su, J. Zhang, Effect of grain size and Cu-rich phase on the electric properties of $CaCu_3Ti_4O_{12}$ ceramics, J. Mater. Sci. 44 (2009) 6149–6154, https://doi.org/10.1007/S10853-009-3850-8/FIGURES/5.

[50] J. Wang, Y. Du, Z. Li, Y. Liu, B. He, C. Cheng, Z. Zhang, Y. Huang, High permittivity and low dielectric loss of (1-x) $Bi_{0.5}(Na_{0.48}K_{0.52})_{0.5}TiO_{3-x}BaZrO_3$ lead-free ceramics, J. Mater. Sci. Mater. Electron. 31 (2020) 10038–10046, https://doi.org/10.1007/S10854-020-03548-8/TABLES/3.

[51] V.L. Gurevich, A.K. Tagantsev, Intrinsic dielectric loss in crystals, Adv. Phys. 40 (1991) 719–767, https://doi.org/10.1080/00018739100101552.

[52] R.G. Munro, S.W. Freiman, Correlation of fracture toughness and strength, J. Am. Ceram. Soc. 82 (2004) 2246–2248, https://doi.org/10.1111/J.1151-2916.1999.TB02069.X.

[53] W.D. Callister, Materials Science and Engineering: an Introduction, 2007, p. 602.